

Review

Indication of Deep-Water Gravity Flow Types by Shelf-Edge Trajectory Migration Patterns: A Case Study of the Quaternary Qiongdongnan Basin, South China Sea

Chang Ma , Hongjun Qu * and Xian Liu

State Key Laboratory of Continental Dynamics, Department of Geology, Northwest University, Xi'an 710069, China; machang0604@foxmail.com (C.M.); liu_xian1996@163.com (X.L.)

* Correspondence: hongjun@nwu.edu.cn

Abstract: The shelf-edge trajectory is comprehensively controlled by tectonics, sediment supply, sea level, and climate fluctuations; its migration and evolution have a strong influence on what happens in the deep-water depositional system during the Quaternary. The shelf-edge trajectory pattern, sediment-budget partitioning into deep-water areas, and reservoir evaluations are focused topics in international geosciences. In this paper, the Qiongdongnan Basin (QDNB) in the northern South China Sea is taken as an example to study how shelf-edge trajectory migration patterns can influence the types of deep-water gravity flow which are triggered there. Through quantitatively delineating the Quaternary shelf-edge trajectory in the QDNB, four types of shelf-edge trajectory are identified, including low angle slow rising type, medium angle rising type, high angle sharp rising type, and retrogradation-slump type. A new sequence stratigraphic framework based on the migration pattern of shelf-edge trajectory is established. There are four (third-order) sequences in the Quaternary, and several systems tracts named lowstand systems tract (LST), transgressive systems tract (TST), and highstand system tract (HST) are identified. This study indicates that the type of deep-water gravity flow can be dominated by the shelf-edge trajectory migration patterns. When the shelf-edge trajectory angle (α) ranged between 0° and 4° , the continental canyons were mostly small-scaled and shallowly incised, with multiple large-scale sandy submarine fan deposits with few MTDs found in the deep-water area. When the angle (α) ranged from $4^\circ < \alpha < 35^\circ$, the size and incision depth of the continental slope canyons increased, relating to frequently interbedded sandy submarine fan deposits and MTDs. When angle (α) ranged from $35^\circ < \alpha < 90^\circ$, only a few deeply-incised canyons were present in the continental slope; in this condition, large-scaled and long-distance MTDs frequently developed, with fewer submarine fans deposits. When angle (α) ranged from $90^\circ < \alpha < 150^\circ$, the valley in the slope area was virtually undeveloped, sediments in the deep-sea plain area consisted mainly of large mass transport deposits, and submarine fan development was minimal. Since the Quaternary, the temperature has been decreasing, the sea level has shown a downward trend, and the East Asian winter monsoon has significantly enhanced, resulting in an overall increase in sediment supply in the study area. However, due to the numerous rivers and rich provenance systems in the west of Hainan Island, a growing continental shelf-edge slope has developed. In the eastern part of Hainan Island, due to fewer rivers, weak provenance sources, strong tectonic activity, and the subsidence center, a type of destructive shelf-edge slope has developed. The above results have certain theoretical significance for the study of shelf-edge systems and the prediction of deep-water gravity flow deposition type.



Citation: Ma, C.; Qu, H.; Liu, X. Indication of Deep-Water Gravity Flow Types by Shelf-Edge Trajectory Migration Patterns: A Case Study of the Quaternary Qiongdongnan Basin, South China Sea. *J. Mar. Sci. Eng.* **2024**, *12*, 2051. <https://doi.org/10.3390/jmse12112051>

Academic Editor: Markes E. Johnson

Received: 30 September 2024

Revised: 7 November 2024

Accepted: 8 November 2024

Published: 12 November 2024



Copyright: © 2024 by the authors. Licensee MDPI, Basel, Switzerland. This article is an open access article distributed under the terms and conditions of the Creative Commons Attribution (CC BY) license (<https://creativecommons.org/licenses/by/4.0/>).

Keywords: shelf-edge trajectory; deep-water sediment gravity flow; the northern South China Sea; Qiongdongnan Basin; Quaternary

1. Introduction

The shelf-edge slope connects the shallow water area of the shelf with the deep-water area of the seabed. The analysis of shelf-edge trajectory involves studying the vertical

and lateral migration process of the shelf-edge slope break point (Figure 1). The shelf-edge trajectory is divided into three types: negative-angle descending type, low-angle slowly ascending type, and high-angle ascending type [1,2]. In recent years, with the continuous development and improvement of the migration theory of shelf edge and slope, the study of shelf-edge trajectory has become an international frontier field of sedimentology and sequence stratigraphy [3–6]. Through the study on the migration types of shelf-edge trajectory, it is believed that the deep-water area of the Porcupine Basin in Ireland has two completely different sedimentary models: one is guided by the formation of canyons and MTDs, and the other is guided by the shelf-edge delta and submarine fans. Pointing out that there is a good response relationship between relative sea level change and shelf-edge migration trajectory [7,8]. Three factors, namely climatic conditions, provenance supply, and accommodative space, are considered to jointly control the shelf margin system and its deep-water response model [5,6,9]. By calculating sediment flux, the relationship between shelf-edge migration trajectory and stratigraphic superposition pattern can be established. A negative-angle descending pattern corresponds to a progradational superposition pattern, a low-angle slowly rising pattern corresponds to a mix between progradative and aggradation superposition patterns, and a high-angle rising pattern corresponds to an aggradational superposition pattern [10,11]. Although sequence stratigraphy itself was also aimed to correlate coastal systems with basins, the analysis of shelf boundary migration trajectory focuses on the continuous sedimentary sequence [12]. By studying the migration trajectory of the shelf edge, the corresponding relationship between it and the deep-sea sedimentary system can be established, and the dynamic dispersion process of sediment and sand bodies can be predicted and analyzed.

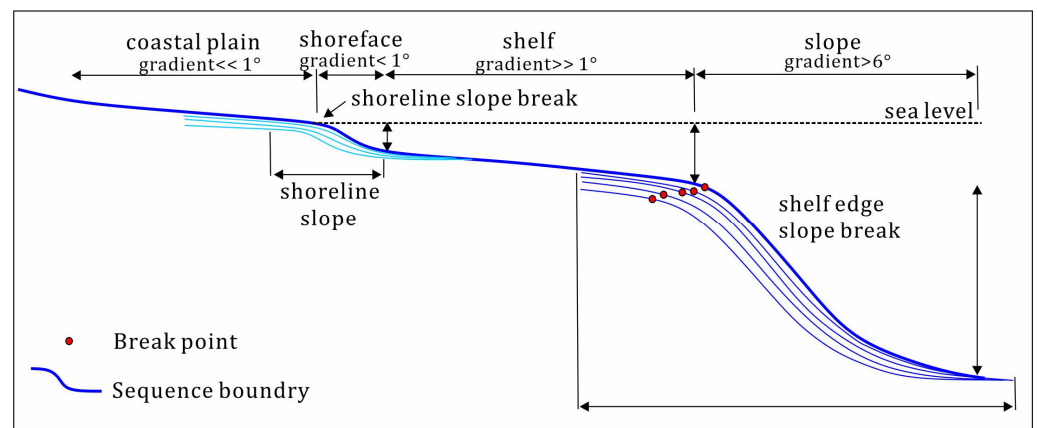


Figure 1. Schematic diagram of shelf-edge slope.

In recent years, the shelf-edge trajectory and connected deep-water system in the QDNB have gradually attracted the attention of scholars [13]. The continental slope of the QDNB can be subdivided into four types: progradation type, slump type, channelized type, and gentle type, with each exhibiting a sequence stacking pattern [14,15]. Based on the quantitative characterization of the types of shelf-edge trajectories and the thickness of sand bodies in each sedimentary unit in the QDNB. It is confirmed that under the condition of constant source supply, the ratio of sand to mudstone in the deep-water plain area corresponding to different types of shelf-edge trajectories is also different. And the angle of the shelf-edge trajectory is inversely proportional to it [5,16]. It is considered that the shelf-edge trajectory of the Quaternary Ledong Formation is mainly a high-angle sharp rising type by using quantitative characterization methods to study the shelf-edge trajectory during the Quaternary in the QDNB [10]. At the same time, it is pointed out that river input, large accommodation, and narrow shelf are the key elements for the development of large-scale sandy submarine fans during this period.

Recently, the broad prospect of natural gas hydrate resources in the deep-water area of the QDNB has been widely discussed [17]. But up to now, there is still a lack of research examples of the shallow Ledong Formation in the QDNB. The lateral difference and evolution of the shelf-edge migration pattern and its relationship with the sedimentary system types in the deep-water area are still unclear. So, we believe that systematic analysis of the migration patterns and evolution of the shelf-edge plays an important role in the prediction of deep-water systems.

2. Geological Setting

2.1. Regional Structural Division

The QDNB, in the northern South China Sea, covers approximately 4.5×10^4 km² with a maximum water depth of the QDNB > 3000 m. With an arc-shaped spreading around Hainan Island with an NE-SW orientation (Figure 2). This sedimentary basin has good hydrocarbon reservoir formation conditions and promising exploration prospects [18]. The QDNB is bounded by the Shenhu Uplift to the east, the Yinggehai Basin and No. 1 Fault to the west, the Yongle Uplift to the south, and Hainan Island to the north [19–21]. From north to south, the basin can be divided into four primary tectonic units, including the Northern Depression Belt, Northern Uplift Belt, Central Depression Belt, and Southern Uplift Belt (Figure 2). The Northern Depression Belt is composed of the Yabei Sag, Songdong Sag, and Songxi Sag. The Central Depression Belt consists of the Yanan Sag, the Ledong Sag, the Lingshui Sag, the Baodao Sag, the Songnan Sag, and the Beijiao Sag [16,22].

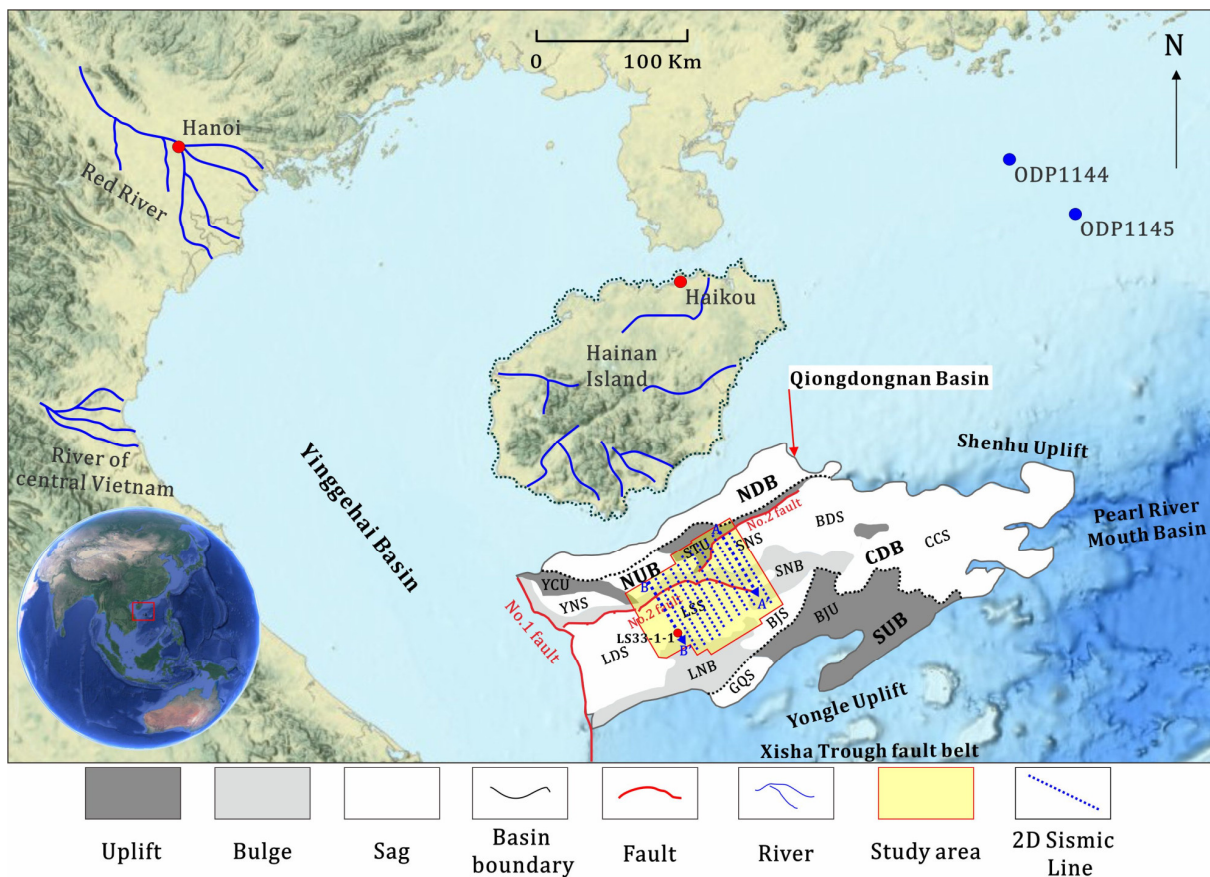


Figure 2. Location of the study area (red polygon). QDNB: Qiongdongnan Basin. SCS: South China Sea. NDB: Northern Depression Belt. CDB: Central Depression Belt. SUB: Southern Uplift Belt YCU: Yacheng Uplift. STU: Songtao Uplift. LNB: Lingnan Bulge. SNB: Songnan Bulge. LDS: Ledong Sag. LSS: Lingshui Sag. YNS: Yanan Sag. BJS: Beijiao Sag. SNS: Songnan Sag. BDS: Baodao Sag. CCS: Changchang Sag. BJU: Beijiao Uplift. GQS: Ganquan Sag.

The study area is located in the Central Depressional Belt, covering approximately 8000 km² (Figure 1). The study area spans the Lingshui Sag and Songtao Uplift to the north, the Lingnan Bulge and Beijiao Sag to the south, the Ledong Sag to the west, and the Songnan Sag and Songnan Bulge to the east. The study area includes a shelf that degrades to a slope and to deep-water bottomsets, has large topographic variations, and the depth of seawater gradually increases from north to south, reaching 2000 m (Figure 2).

2.2. Structural Evolution and Sedimentary Filling

The formation of the QDNB is closely related to the complicated interactions among the Indo-Australian Plate, Eurasia Plate, Pacific Plate, and the opening of the SCS [23]. Four regional tectonic movements in the Cenozoic period influenced the stages of tectonic evolution of the basin [24]: (1) the Shenhu movement in the Late Cretaceous–Paleocene, (2) the South China Sea movement in the Eocene–early Oligocene, (3) the South China Sea seabed spreading in the late Oligocene–middle Miocene, and (4) the Dongsha movement in the late Miocene to Quaternary. According to previous studies, the rifting of the QDNB may have started in the Eocene [19]. Since the Eocene, the basin has undergone two major stages of tectonic evolution: rifting and post-rifting depression, leading to a two-layer structure characterized by an “upper depression and lower fault” [21]. Seismic horizon T60, interpreted as a major tectonic event (Figure 3), is used to divide the basin into two major tectonic layers, namely, upper and lower, which represent the products of the rifting and post-rifting subsidence stages, respectively. Combined with the characteristics of extensional fracturing in the basin, they can be further divided into the pre-rifting stage, the syn-rifting stage, the thermal subsidence stage, and the accelerated subsidence stage [24,25].

High sedimentation rates result in Cenozoic sediment thicknesses ranging from 3000 to 16,000 m [21,26,27]. The stratigraphic sequence is subdivided into eight formations based on the drilling and seismic horizons (Figure 3). The Lingtou Formation is undrilled and is interpreted to represent Eocene lacustrine sedimentary facies; this formation is an important hydrocarbon source rock based on seismic data interpretation [28]. The Yacheng Formation was deposited in the early Oligocene and contains marsh–coastal plain facies [29]. This formation is widely considered to be the main hydrocarbon source rock of the Lingshui 17-2 gas field [30]. The Lingshui Formation contains coastal facies that were deposited in the late Oligocene [18]. The T60 unconformity is the boundary between the Lingshui Formation and the Sanya Formation (coastal shallow marine facies). The Meishan and Huangliu Formations were deposited in the middle and late Miocene and contain shallow to deep coastal facies [31]. The Huangliu Formation sands may be the hydrocarbon reservoir of the QDNB [18]. T20 is the boundary between the Yinggehai Formation and the Ledong Formation (Quaternary), which contains bathyal to abyssal sedimentary facies dominated by fine-grained sediments [18]. Since the Quaternary, there have been three major source areas in the QDNB, namely, the Red River provenance, the Hainan Island provenance, and the central Vietnam provenance. In the early Quaternary, the supply of sediments of the Red River was weak, which only affected the northwestern shelf area of the QDNB. The provenance of central Vietnam has always affected the middle part of the basin, and almost the whole basin is under the influence of the provenance of Hainan Island. During the late Ledong Formation (0.8 My~present), the source of the Red River was greatly strengthened, and the influence range could reach the middle part of the basin. At the same time, the intensity of supply in central Vietnam was slightly reduced, and the influence range was smaller than that of the early Quaternary. The sediment supply from Hainan Island still occupies a dominant position [20,32,33] (Figure 3).

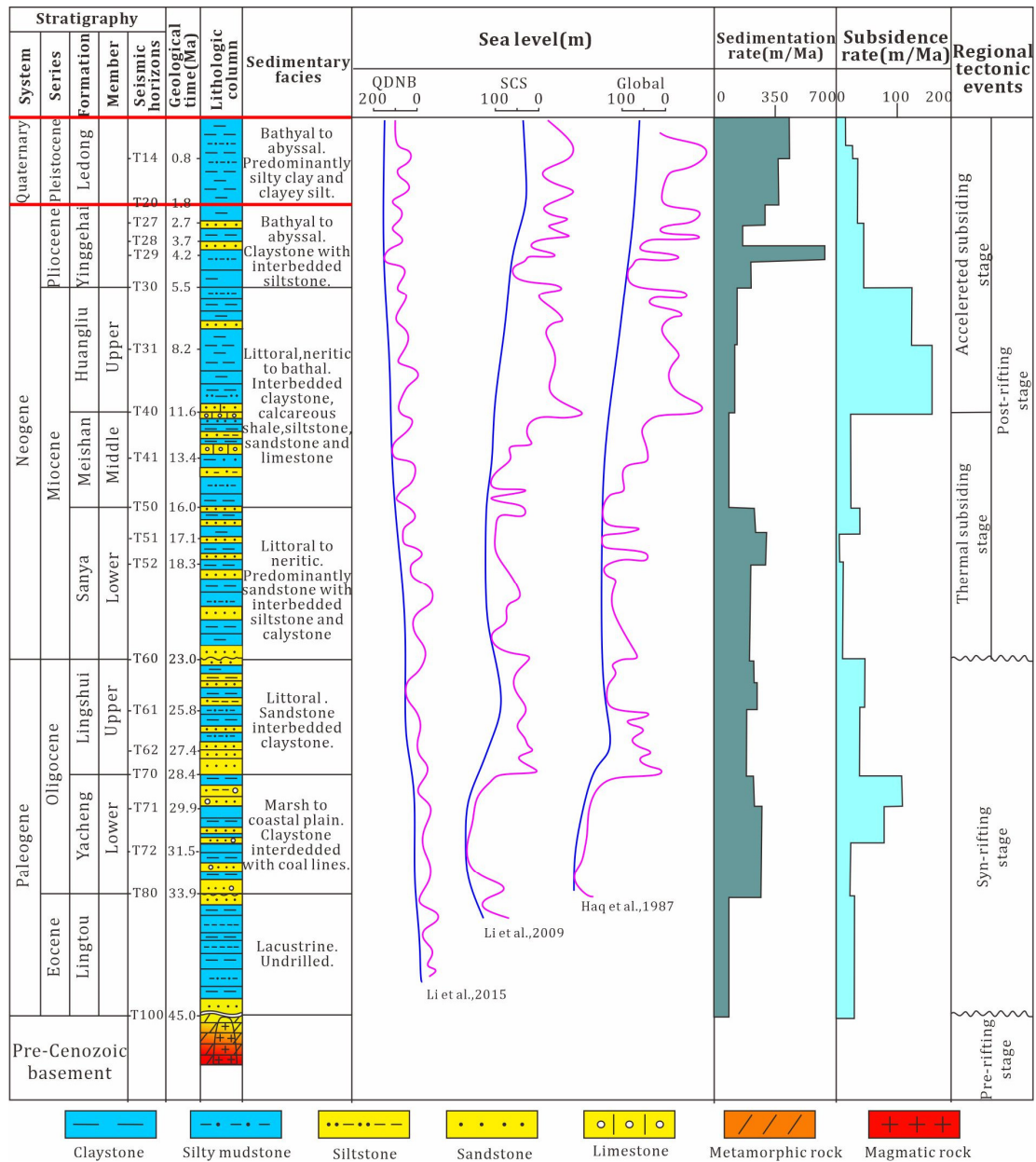


Figure 3. Comprehensive stratigraphic column of the QDNB (modified from [34,35]. The sedimentation rate and subsidence rate are redrawn after [27,36]. Sea level curves are derived from [37–39]. QDNB: Qiongdongnan Basin. SCS: South China Sea.

3. Data and Methods

3.1. Data

In this study, seismic stratigraphy was applied to analyze the shape and trajectory angle of the continental slope of the QDNB. The study area was crossed by 2D seismic data from 113 seismic lines and covered approximately 10,000 km² with high density (Figure 2). The frequency was nearly 38 Hz in the interval of interest, providing a vertical resolution of 20 to 30 m, and the seismic wave velocity was 1700 m/s.

Twelve along shelf-slope (north-west/south-east) seismic lines were selected for data statistics and analysis, and two seismic lines (AA' and BB') were used for detailed sequence stratigraphic analysis integrated with either well data (LS33-1-1). Line L1 (AA') is located in the western part of the basin, and Line L2 (BB') is located in the eastern one (Figure 2).

These lines represent the characteristics of two different types of continental slopes in the study area.

3.2. Methods

The shelf-edge trajectory migration is composed of a series of slope breakpoints, which record the development and evolution of the shelf edge (Figure 4). Its morphology can be characterized by the following parameters [7]: (1) accretion distance and progradation distance between the shelf edge, (2) accretion rate and progradation rate, (3) sediment flux, (4) shelf-edge trajectory angle, (5) horizontal distance and vertical distance between slope break point and slope toe point, and (6) slope topography angle.

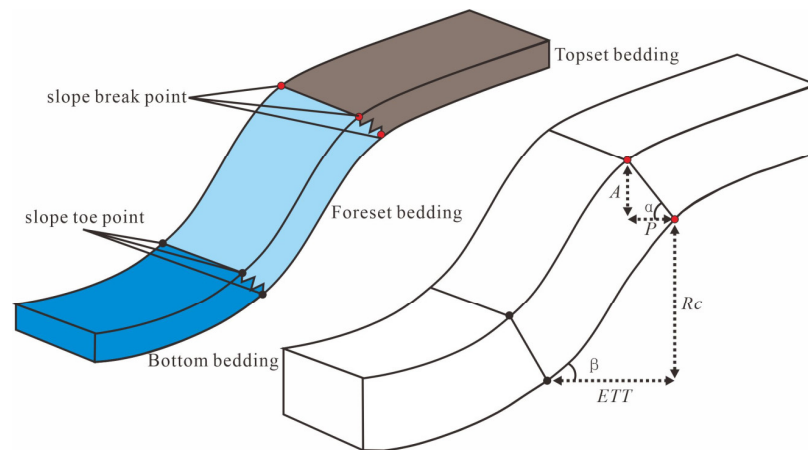


Figure 4. A model for calculating the shelf-edge trajectory (α), the shelf-edge migration (P), the vertical distance between the successive shelf edges (A), the height (in m) between the toe and the shelf edge (R_c), the edge-to-toe distance (ETT), and the slope angle (β).

The shelf-edge trajectory angle (α) can be calculated as:

$$\alpha \text{ (degree)} = \tan^{-1} (A/P)$$

where α is the shelf-edge trajectory angle (in degrees), A is the height between successive shelf edges (in m) and P is the length of the shelf-edge migration (in m).

The slope angles are calculated as:

$$\beta \text{ (degree)} = \tan^{-1} (R_c/ETT)$$

where β is the slope angle (in degrees), R_c is the height (in m) between the toe and the shelf edge and ETT is the edge-to-toe distance (in m).

Accretion rate (R_a), progradation rate (R_p), and sediment flux (F_c) cross sections at each stage can be calculated as:

$$R_a = A/T$$

$$R_p = P/T$$

$$F_c = R_p \times A \times 10^{-3}$$

R_a is the accretion rate (in m/My), A is the height between successive shelf edges (in m), and T is the time of the shelf-edge migration (in My). Additionally, R_p is the progradation rate (in m/My), P is the length of the shelf-edge migration (in m), T is the time of the shelf-edge migration (in My), F_c is the sediment flux (in m^3/My), R_p is the progradation rate (in m/My), and A is the height between successive shelf edges (in m) (Tables S1–S3). Although the current trajectory angle measurement method of shelf edge has high accuracy, how to correctly statistical accretion and progradation rate is still a challenge.

Based on the comparison of previous research data, the coupling relationship between sea and land development, relative sea level fluctuation, and sediment supply was established. Thus, how these mechanisms control various types of stacking patterns and parameters could also be determined.

4. Results

4.1. Sequence Stratigraphic Framework

According to classical sequence stratigraphy combined with the relative change of sea level in QDNB [40,41], the sequence boundary is identified by using typical seismic termination relations including upper exceedance, top exceedance, lower exceedance, and local cutting. By using this method, and combining gamma-ray logs and lithology, five sequence boundaries and four third-order sequences (S1, S2, S3, and S4) were identified (Figure 5).

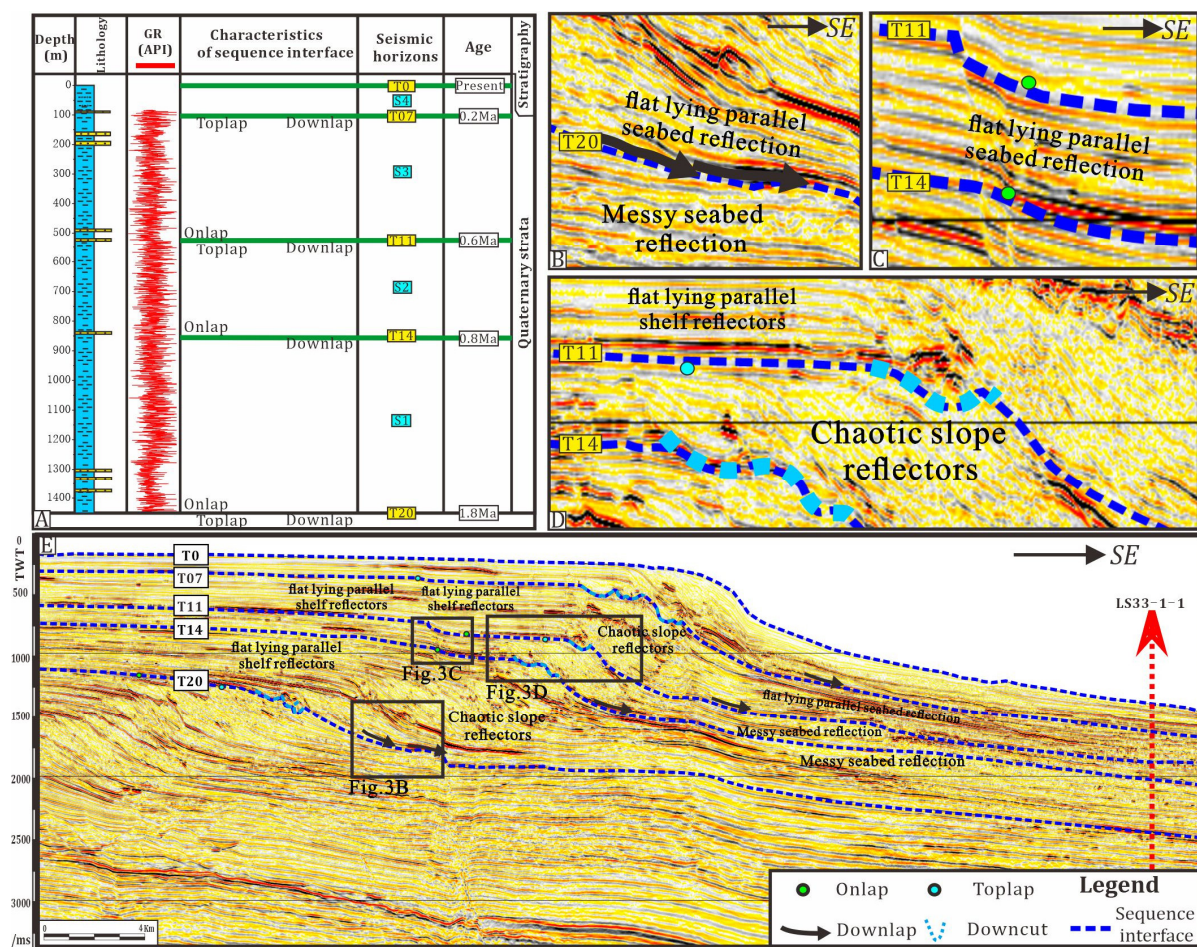


Figure 5. Sequence stratigraphic framework established from the deep-water well LS33-1-1 in the QDNB. (A) Lithology and well-logging data of LS33-1-1. (B–D) Typical seismic contact relationship. See (E) for the locations of (B–D). (E) 2D seismic profile across the study area. See Figure 1 for the locations of LS33-1-1 and (E) QDNB: Qiongdongnan Basin.

The lithology changes above and below the T20 sequence boundary, with sandstone above the sequence boundary and mudstone below the sequence boundary. GR log curve (Figure 5) is abnormally small at the sequence boundary, showing a zigzag bell shape above the sequence boundary and a zigzag box shape below the sequence boundary. The lithology changes above and below the T14 sequence boundary, with fine sandstone above the sequence boundary and mudstone below the sequence boundary. The GR curve is

abnormally small at the sequence boundary (Figure 5), showing a zigzag bell shape above the sequence boundary and a zigzag box shape below the sequence boundary. The lithology changes above and below the T11 sequence boundary, with mudstone above the sequence boundary and thin sandstone below the sequence boundary. The GR curve is abnormally small at the sequence boundary (Figure 5), and the upper and lower parts of the sequence boundary are sawtooth bell-shaped. The T07 sequence boundary is dominated by medium-weak amplitude and medium-high continuous seismic reflection in the shelf area, and a typical onlap can be seen. The shelf-edge deposits are mainly progradated, and the formation thickness is small (40~90 m). In the slope area, the main axis is the medium-high amplitude and low-continuous seismic reflection, and local top superimposed and truncated structures can be seen. The deep-water area shows a meso-strong amplitude and medium-continuous type of sheet seismic reflection, with a wide range of lower superstructures above the sequence boundary, and large-scale seismic in-phase axes of strong amplitude, high continuity, and medium frequency can be seen. T0 is the seabed (Figure 5).

The shelf edge of Sequence S1 (T20-T14) is characterized by parallel progradation and accretion. The progradation distance and the strata thickness are both large in the northwest of the basin, and the accretion and progradation are both clearly recognizable. The thickness is small in the northeast of the basin, with accretion and progradation occurring mainly in small amounts. Strong amplitude and high continuous seismic in-phase axis can be seen in the continental shelf area. The continental slope area is dominated by a set of thick shelf-edge delta. In the deep-water area, chaotic reflection structures can be seen with massive medium-strong amplitude reflections, which are MTDs; on the other hand, parallel reflections of weak amplitude and high continuity are widely seen, mainly in the mudstone deposits (Figure 5).

The eastern shelf edge and shelf edge of sequence S2 (T14-T11) are characterized by strong accretion. The strata in the northwest of the basin are thick and the progradation is obvious. In the northeast, the stratum thickness is thin and accretion is dominant. In the continental shelf area, strong amplitude and high continuous seismic in-phase axis can be seen, and a large number of continental shelf waterways are developed. The continental slope area is dominated by the marginal delta of the shelf and the valley of the slope. In the deep-water area, multi-stage MTDs can be seen stacked on top of one another, with parallel reflections of weak amplitude and high continuity widely developed, mainly in the mudstone deposits (Figure 5).

The shelf edge of Sequence S3 (T11-T07) is characterized by strong accretion, and the strata are thick in the west and thin in the east. The continental shelf area is dominated by strong amplitude and high continuous seismic in-phase axis, and the continental shelf channel is more developed. The continental slope area is dominated by the MTDs formed by the delta collapse at the edge of the shelf and the MTDs from the inner wall of the slope canyon. Multi-stage large-scale MTDs can also be seen in the deep-water area; the flow direction is mainly southeast, and a large number of weak amplitude, high continuous type of parallel reflections are also developed, which are mainly mudstone deposits (Figure 5).

The shelf edge of Sequence S4 (T07-T0) is characterized by strong accretion, and the strata inherit the characteristics of thick west and thin east. The continental shelf delta plain is widely distributed in the continental shelf area. The northwestern continental slope area is dominated by shelf-edge delta deposits with a large number of MTDs, and the northeast is dominated by slope canyon development with a large number of MTDs. The deep-water plain area is dominated by chaotic reflection structures, mainly large MTDs (Figure 5).

4.2. Types of Shelf-Edge Migration

Based on the statistical analysis of the parameters of the shelf-edge trajectory of 12 typical seismic profiles in the study area, the Quaternary shelf-edge trajectory in QDNB is classified into the following four types:

(1) Low-angle slow rising type shelf-edge trajectory: The accretion distance of this type of shelf-edge trajectory ranges from -50 to 100 m, and the progradation distance of the four types of shelf-edge trajectory is the smallest. The accretion distance ranges from 0 to 8000 m, the ratio of accretion distance to progradation distance is -0.01 to 0.07 (Figure 6A and Table S1), and the angle of the shelf-edge trajectory is -1 to 4° (Figure 6B). The shelf-edge slope height is 350 to 680 m and the length is 3800 – $11,000$ m, which is the longest among the four shelf-edge trajectory types, and the slope toe angle is 2.5 to 9° (Table S2).

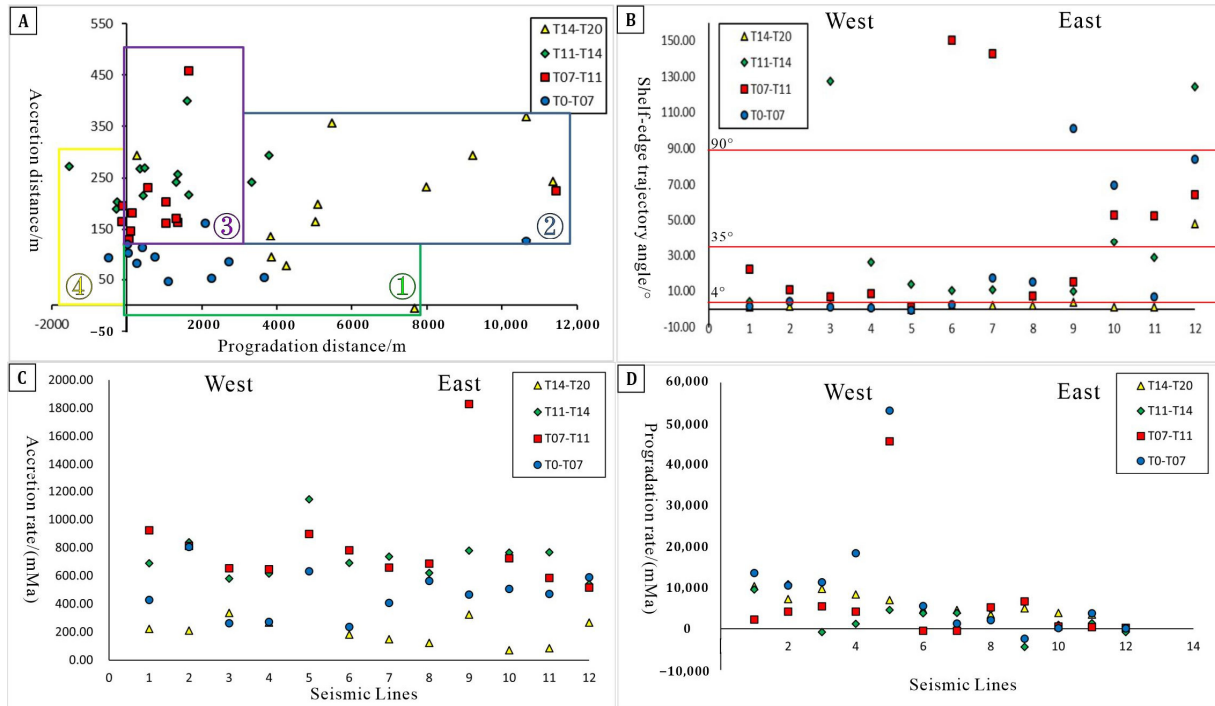


Figure 6. (A) The intersection between accretion distance and progradation distance at the edge of the Quaternary shelf in QDNB (The numbered colored boxes represent the parameter range (accretion and progradation distance) of the shelf-edge trajectory); (B) Shelf-edge trajectory angle statistics of each section of the Quaternary in QDNB; (C) Accretion rate statistics of each section of the Quaternary in QDNB; (D) Progradation rate statistics of each section of the Quaternary in QDNB.

(2) Medium-angle rising type shelf-edge trajectory: The accretion distance of this type of shelf-edge trajectory is between 100 to 400 m, and the progradation distance is about 300 to $12,000$ m (Figure 6A and Table S1). Compared with type (1), the accretion distance and progradation distance are larger, the ratio of accretion distance to progradation distance is 0.07 to 0.55 , and the angle of the shelf-edge trajectory is 4 to 35° (Figure 6B). The height of the slope at the edge of the shelf is 200 – 570 m, the length is 200 – $10,500$ m, and the angle of the slope toe is 2 to 7° (Table S2).

(3) High-angle sharp rising type shelf-edge trajectory: The accretion distance of this type of shelf-edge trajectory is between 100 to 500 m, which is the largest among the three types of shelf-edge trajectory, and the progradation distance is 0 to 3000 m (Figure 6A and Table S1). The ratio of accretion distance to progradation distance is 0.76 to 9.45 , the shelf-edge trajectory angle is between 35 to 90° (Figure 6B), the slope height of the shelf edge is between 200 to 600 m, the length varies between 3000 to 8000 m, and the slope toe angle is 3 to 7° (Table S2).

(4) Retrogradation-slump type shelf-edge trajectory: The accretion distance of this type of shelf-edge trajectory is between 0 – 300 m, and the progradation distance is -2000 – 0 m (Figure 6A and Table S1), which is the smallest among the four types. The ratio of accretion distance to progradation distance is less than 0 , the shelf-edge trajectory angle is between

90–150° (Figure 6B), the slope height of the shelf edge is in the range of 350–550 m, the length varies little in the range of 3000–8000 m, and the slope toe angle is 3–6° (Table S2).

4.3. Migration and Evolution of Shelf-Edge Trajectory

4.3.1. S1 (T20-T14)

S1 is characterized by strong accretion, progradation, and high sediment flux (Table S3), and most of shelf-edge trajectories are low-angle slow rising types. The accretion distance of the shelf edge ranged from −4 to 369.5 m, with an average value of 204.85 m. The shelf-edge progradation distance is in the range of 262.5 to 11,362.5 m, with an average of 6221.88 m (Figure 6A). Most of the shelf-edge trajectory angles are between 0 and 4°. The slope height ranged from 282.36 to 575.2 m, with an average value of 455.9 m. The slope length is in the range of 3850 to 8625 m, with an average value of 6457.5 m. The slope angle is between 2 and 6° (Table S2).

The accretion rate of the northwestern shelf edge ranges from −4 to 350 m/My, and the accretion rate ranges from 6900 to 10,500 m/My. The accretion rate of the northeastern shelf edge is between 70 and 270 m/My, and the accretion rate is between 230 and 3800 m/My. The sediment flux in the northwest is in the range of −33 to 3500 m³/My, the sediment flux in the middle is in the range of 450 to 1800 m³/My, and the sediment flux in the northeast is in the range of 70 to 330 m³/My (Table S3). The sediment flux decreased gradually from west to east during this period, indicating a decline in source activity from west to east (Figure 7).

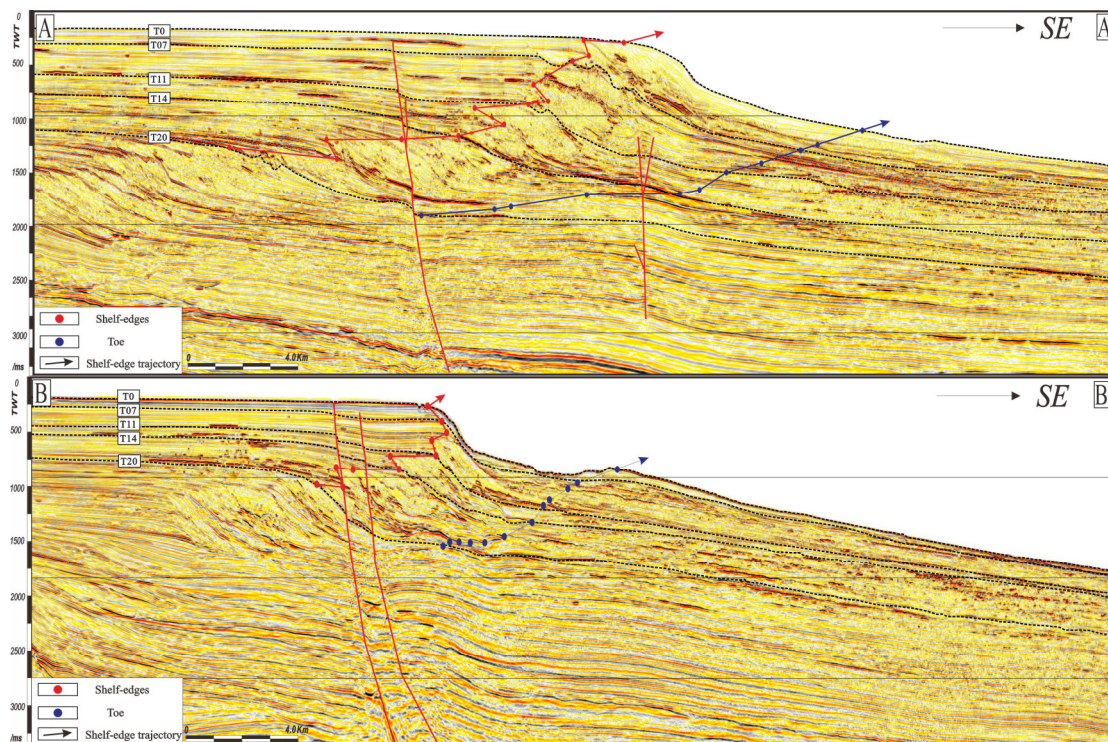


Figure 7. Two seismic sections (AA' and BB') which shown the shelf-edge migration trajectories, see locations in Figure 1. Shelf edges and toes are marked by red and blue dots, respectively.

4.3.2. S2 (T14-T11)

S2 is characterized by strong progradation and high sediment flux (Table S3), and most of the shelf-edge trajectories on the northwestern are low-angle slow rising types, or medium-angle rising types. Most of the trajectories of the northeastern shelf edge are of high-angle sharp rising type.

The accretion distance of the shelf edge ranges from 400.5 to 188.96 m, with an average value of 255.72 m. The shelf-edge progradation distance is in the range of −1537 to 3800 m,

with an average of 1023.96 m (Figure 6A). In the northwestern region, the trajectory angle of the shelf edge is between 4 and 35°. In the northeastern region, the trajectory angle of the shelf edge increases rapidly, with a variation range of 30 to 40°. There are also a few retrogradation-slump type shelf-edge trajectories, with angles between 100 and 130°. The slope height ranges from 270.88 m to 520.92 m, with an average value of 391.57 m. The slope length is in the range of 2125 to 8300 m, with an average of 5387.5 m. The slope angle is between 2 and 8° (Table S2).

The accretion rate of the northwestern shelf edge ranges from 579.09 to 1144.11 m/My, and the progradation rate ranges from −750 to 10,857.14 m/My. The accretion rate of the middle shelf edge ranges from 600 to 800 m/My, and the progradation rate ranges from −4392.86 to 4750 m/My. The accretion rate of the northeastern shelf edge is between 500 and 800 m/My, and the progradation rate is between −785.71 and 1392.86 m/My. The sediment flux in the northwest is in the range of −152.01 to 3188.96 m³/My, and the sediment flux in the northeast is in the range of −148.47 to 374.12 m³/My (Table S3). The progradation rate gradually decreased from west to east during this stage. The sediment flux decreased gradually from west to east, and the sediment flux increased slightly in S2 compared with that in S1, indicating that the provenance supply in this stage inherited the characteristics of “strong in west and weak in east” in S1 (Figure 7).

4.3.3. S3 (T11-T07)

S3 is characterized by strong accretion, weak progradation, and sediment flux (Table S3). Most of the shelf-edge trajectories in the northwest are a medium-angle rising type, and few retrogradation-slump types are caused by slumps. Most of the northeastern shelf-edge trajectories are high-angle sharp rising types.

The accretion distance of the shelf edge ranges from 129.2 to 457.6 m, with an average value of 202.72 m. The shelf-edge progradation distance is in the range of −125 to 11,437.5 m, with an average value of 1541.67 m. In the northwestern region, the shelf-edge trajectory angle is between 1 and 23°. In the northeastern region, the shelf-edge trajectory angle increases rapidly, with a variation range of 52 to 65°. There are also a few retrogradation-slump type shelf-edge trajectories, with angles between 100 and 130°. The slope height ranges from 381.2 to 585.28 m, with an average value of 458.59 m. The slope length is in the range of 3200 to 8800 m, with an average value of 7073.96 m. The slope angle is between 2 and 8° (Table S2).

The accretion rate of the northern shelf edge ranges from 646.24–924.8 m/My, and the progradation rate ranges from 2250–45,750 m/My. The accretion rate of the northeastern shelf edge is between 516.8–725.6 m/My, and the progradation rate is between 250–550 m/My. The sediment flux in the northwest is in the range of 520.2–10,266.3 m³/My, and the sediment flux in the northeast is in the range of 32.3–99.77 m³/My (Table S3). The accretion rate decreased from west to east during this stage. The rate of accumulation gradually decreased from west to east. Sediment flux decreased significantly from west to east. However, compared with S2, the sediment flux decreased slightly. It shows that although the source supply of S2 in the west is more powerful than east, it has a decreasing trend in general (Figure 7).

4.3.4. S4 (T07-T0)

The northwestern part of S4 is characterized by strong progradation and high sediment flux. The northeastern part is characterized by strong accretion, weak progradation, and low sediment flux (Table S3), while the northwestern part of the shelf edge is mostly low-angle slow rising type, and most of the trajectories of the northeastern shelf edge are of high-angle sharp rising type. There also the retrogradation-slump type caused by the slump.

The accretion distance of the shelf edge ranged from 47.4–126.68 m, with an average value of 94.12 m. The shelf-edge progradation distance ranges from −475–10,650 m, with an average value of 1960.42 m. In the northwestern region, the shelf-edge trajectory angle

is between 0 and 4°. In the northeastern region, the shelf-edge trajectory angle increases rapidly, with a range of 60–90°. There are also a few retrogradation-slump type shelf-edge trajectories with an angle of 101°. The slope height ranged from 390.28 to 647.96 m, with an average value of 543.67 m. The slope length was in the range of 3500–10,537.5 m, with an average value of 7410.42 m. The slope angle is between 3–9° (Table S2).

The accretion rate of the northwestern shelf margin ranges from 263.4–805.6 m/My, and the progradation rate ranges from –10,500–53,250 m/My. The accretion rate of the northeastern shelf edge is between 472.2–590.6 m /My, and the progradation rate is between 62.5–3812.5 m /My. The sediment flux in the northwest is in the range of 595.94–6745.71 m³/My, and that in the northeast is in the range of 7.38–360.05 m³/My (Table S3). The deposition rate and sediment flux decreased significantly from west to east during this stage, with the sediment flux showing a decreasing trend compared with S3. It shows that the provenance supply in this stage inherited the characteristics of “strong in the west and weak in the east” in the S3 stage and continued to decrease (Figure 7).

4.4. Types of Gravity Flow Deposits in Deep Water

4.4.1. Submarine Fan

The submarine fan is an element of the basin architecture that is composed of the varied types of deposits [42]. In the plane, it is foliated, and in the section, it is a flat hill with bidirectional downward superposition; in the fan body, it is a parallel and sub-parallel structure, showing the reflection characteristics of high continuity and strong amplitude [43].

In the northwestern part of the study area, the submarine fan develops on a large scale, with a width of 8 to 12 km and a thin thickness, fluctuating between 25 to 30 m. The northeast submarine fan has a small distribution scale, with a width between 6 and 10 km and a thickness between 25 and 30 m (Figure 8).

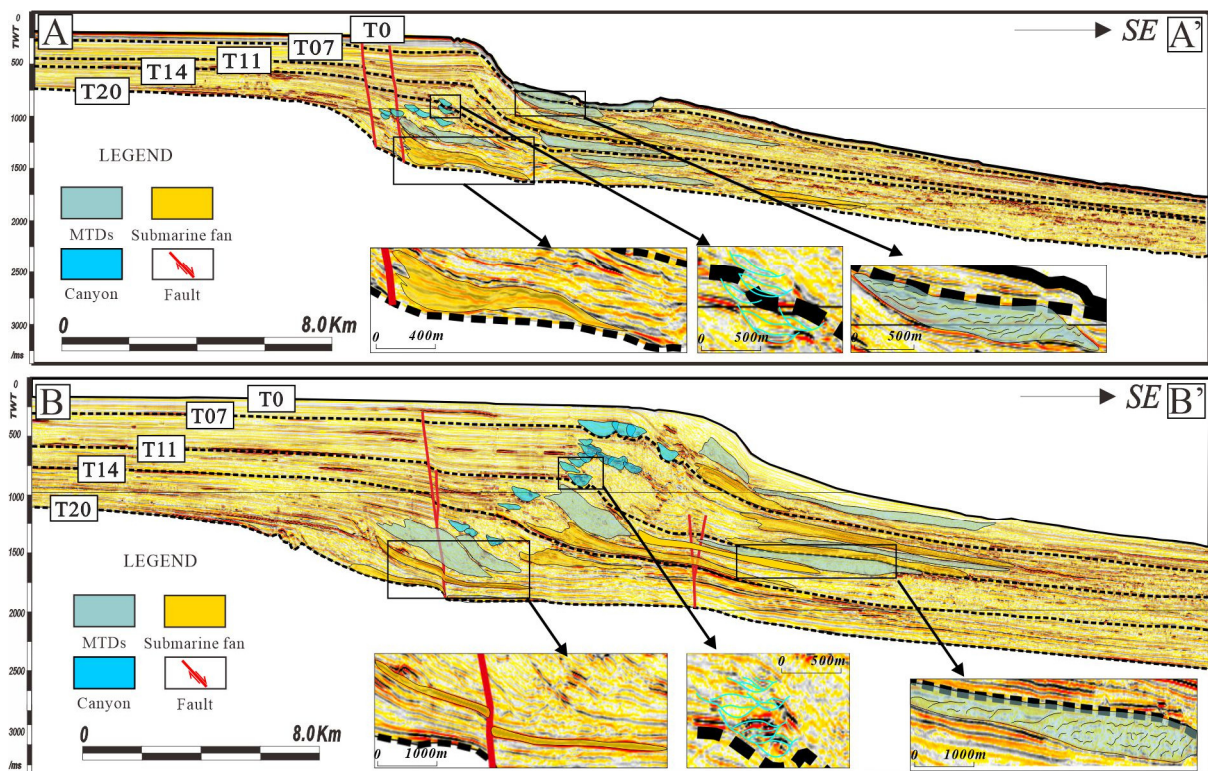


Figure 8. Sedimentary types of gravity flow are shown in seismic sections (AA' and BB') in the QDNB. See locations in Figure 1.

4.4.2. Mass Transport Deposits

Mass transport deposits (MTDs) are a kind of event deposits formed by the instability and collapse of continental slope sediments [44,45]. There is a chaotic reflection on the profile, and residual blocks retaining the original formation information can be seen inside. The thrust fault can be seen on the toe, with poor continuity and weak amplitude reflection characteristics (Figure 8).

The orientation of MTDs in the study area is mainly from the northwest to the southeast, and the primary block is the main component near the continental slope, while the clastic flow is the main component near the submarine plain. They are superimposed on each other, the overlying MTDs erode the underlying layer evidently, the thrust fault can be seen, and the shear plane between MTDs is evident (Figure 8).

4.4.3. Canyon Filled Deposit

The canyon is the conduit through which sediment is transported from the shelf to the deep-sea basin [46,47]. Its cross-section is a "U" or "V" shape; the "U" shape is mainly filled by debris flow deposits, and the "V" shape is mainly filled by muddy deposits, and its internal structure is complex and diverse due to different sediments. Most of the canyons in the study area have chaotic internal structures with weak continuity and moderate-weak amplitude reflection characteristics, and the interior is filled with debris flow deposits or deep-sea mud deposits, and the block of canyon wall collapses. Therefore, it is considered that the canyon-fill deposits are mainly gravity flow or deep-sea mud deposits (Figure 8).

Since 0.8 My, a large number of canyons have developed in the study area, with an average cutting depth of 60 m and an average width of 90 m. The northwestern canyons are mostly characterized by lateral tangential overlapping relationships, while the northeastern canyons are characterized by vertical tangential overlapping relationships (Figure 8).

5. Discussion

5.1. *The Evolution of Systems Tract Indicating by the Shelf-Edge Trajectory*

The relationship between relative sea-level change and sediment supply may lead to different sequence accumulation patterns and shelf margin trajectories [48–52]. Due to the response of the shelf edge to the changes in sediment supply and relative sea level change, it presents a descending, rising, or flat trajectory [6,7,9]. This suggests that the sedimentary environment can be distinguished based on the shelf-edge trajectory, and thus corresponding system tract types can be inferred. The observed patterns are discussed below [49,53].

5.1.1. Lowstand Systems Tract (LST)

During this time, the relative sea level began to rise from the lowest point, and the shelf-edge trajectory was medium-angle rising type, which had the characteristics of medium accretion and weak accretion. The topset bedding is medium thick, the foreset bedding is thin, and the bottom bedding is thin, indicating that sediments are still transported to the basin, but submarine fan deposits are easily formed near the slope of the shelf edge due to rising sea level (Figure 9).

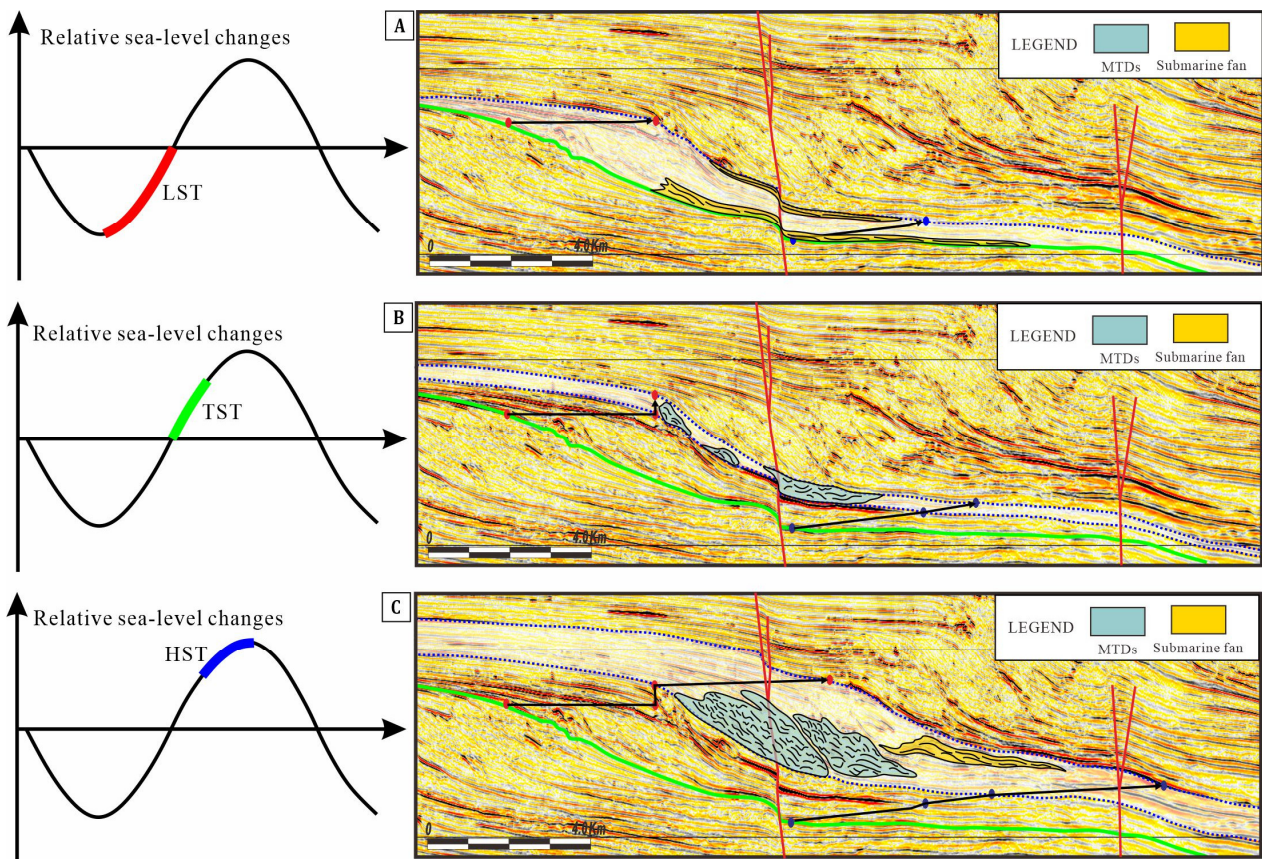


Figure 9. Relationship between relative sea level and shelf-edge trajectories. Three combinations of the shelf-edge trajectories with the corresponding stages of sea-level fluctuation. (A) LST has more submarine fans, (B) TST has more MTDs, and (C) HST has both of submarine fans and MTDs.

5.1.2. Transgressive Systems Tract (TST)

During this time, the relative sea level rose rapidly, and the shelf-edge trajectory angle was retrogradation-slump type, which was characterized by strong regression and forced accumulation. The thickness of the topset bedding is medium, the foreset bedding is thin, and the bottom bedding is thin, indicating that sediments accumulate rapidly at the shelf edge due to the rapid rise of sea level and retreat of the source. It could easily become instable and collapse, forming MTDs (Figure 9).

5.1.3. Highstand System Tract (HST)

During this time, the relative sea level rise rate slowed down, and the shelf-edge trajectory angle was low-angle slow rising type or high-angle sharp rising type, which had the characteristics of strong prograde and forced prograde. The thickness of the topset bedding, foreset bedding, and bottom set bedding are large, indicating that the sediment supply is strong, and the submarine fan and MTDs are superimposed near the slope of the shelf edge (Figure 9).

Based on the research results, in seismic data interpretation, we should pay more attention to finding favorable reservoir groups at the sequence interface (HST) or under the sequence interface. Fans developed above the sequence interface (LST) tend to have longer transport distances and thinner thicknesses, while fans cultivated under the sequence interface (HST) have shorter transport distances and larger thicknesses.

5.2. Relationship Between Shelf-Edge Migration and Deep-Water Gravity Flow Deposition

During the S1 (1.8 Ma to 0.8 Ma), the overall trajectory of the shelf edge was dominated by a low-angle and slow-rising type (Figure 10), and the sediment supply rate in the

northwest was greater than that in the northeast. A large volume of submarine fan deposits with low thickness and the short transport distance was present in the northwest. In contrast, the submarine fan is less developed in the northeast, with thin thickness, a small width, and a long transport distance. There were fewer canyons in the northwest and more in the northeast. Some MTDs are developed in the slope area (Figure 10).

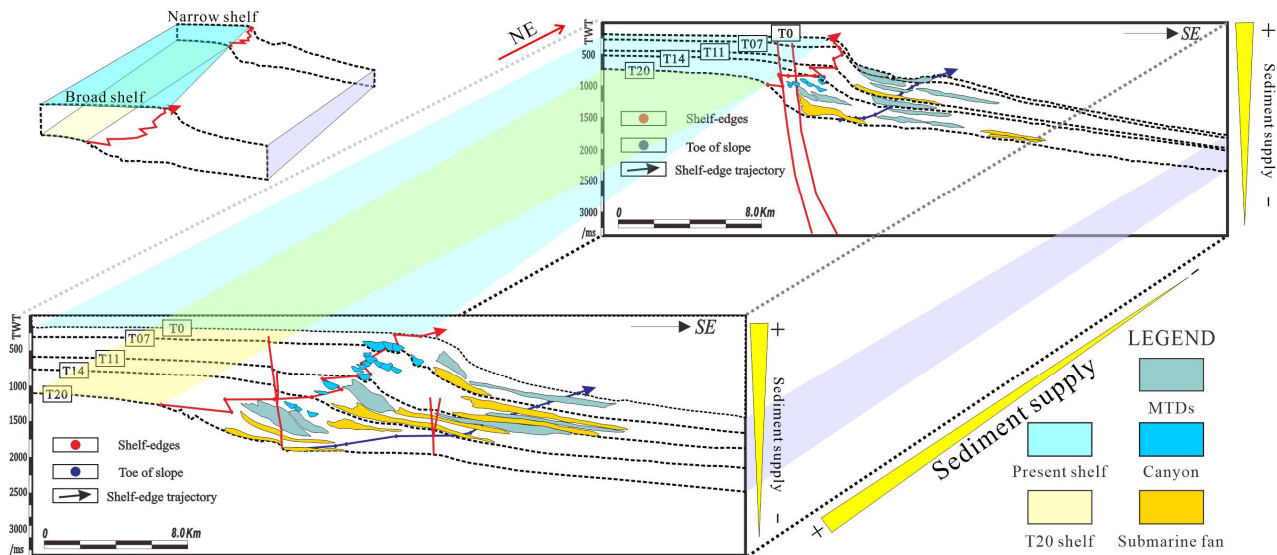


Figure 10. Response mode of deep-water deposition to shelf-edge trajectory in the Quaternary Qiongdongnan Basin. The western shelf margin is dominated by progradation, while the eastern shelf margin is dominated by accretion.

During S2 (0.8 Ma to 0.6 Ma), the shelf-edge trajectory in the northwest was dominated by the low-angle slow rising type, while that in the northeast was dominated by the medium-angle rising type (Figure 7). The sediment supply rate in the northwest was still higher than that in the northeast. There were more submarine fan deposits in the northwest, which had a certain inheritance, but less in the northeast. Canyons were more developed in the northwest but less in the northeast. A small number of MTDs developed in the northwest and thin layers developed in the northeast (Figure 10).

During S3 (0.6 Ma to 0.2 Ma), the northwest shelf-edge trajectory was dominated by medium-angle rising type, and the northeast shelf-edge trajectory was mainly of the high-angle sharp rising type. The development scale of submarine fans in the northwest have a long transport distance, while only a few submarine fans developed in the northeast. MTDs and submarine fan deposits overlapped and more MTDs developed in the northeast at this time (Figure 10). During this time, with the increase of the shelf-edge trajectory angle, the development of submarine fan sediments began to decrease, while the development of MTDs increased.

During the S4 (0.2 Ma to present), the northwest shelf-edge trajectory was dominated by the medium-angle rising type, and the northeast shelf-edge trajectory was dominated by the high-angle sharp rising type. The development scale of submarine fan in the northwest was the smallest, canyons developed extensively, and MTDs and submarine fan overlapped. In the northeast, there was almost no submarine fan deposition, no canyon development, and large-scale development of MTDs (Figure 10). During this time, with the increase of the shelf-edge trajectory angle, the development of submarine fans began to decrease, and MTDs began to develop on a large scale.

Based on what has been mentioned above, it is concluded that the shelf-edge trajectory is a record of the changes in sea level, which also can indicate the development of the depositional system in the basin. When the shelf-edge trajectory angle is $-1^\circ < \alpha < 4^\circ$, the canyon size in the slope area is small and the downcutting is shallow, and the deep-sea

plain area has multi-stage large-scale submarine fan deposits with fewer MTDs. When $4^\circ < \alpha < 35^\circ$, the canyon size increases in the continental slope area, and both submarine fan deposits and MTDs appear in the deep-sea plain area. When $35^\circ < \alpha < 90^\circ$, the valley in the continental slope area is less developed but deep cut, the sediments in the deep-sea plain area are mainly large MTDs, and the submarine fan is rarely developed. When $90^\circ < \alpha < 150^\circ$, the valley in the continental slope area is almost undeveloped, the sediments in the deep-sea plain area are mainly large MTDs, and the submarine fan is nearly undeveloped (Figure 10).

5.3. Shelf-Edge Trajectory Driven by Multiple Factors

5.3.1. Influence of Relative Sea Level Change on Shelf-Edge Trajectory

(1) Tectonic subsidence

At 10.5 Ma, the subduction of the Pacific plate and the Eurasian plate, the right-lateral strike-slip action of the Red River fault, and the regional activity of Fault No. 2 caused the subsidence center to shift eastward, and the topography of the basin showed the characteristics of high in the west and low in the east, which has continued to the present day [20,54]. Since the Quaternary, the sedimentation rate of the QDNB peaked [55], and the difference between the sedimentation rates of the east and west part of the QDNB affected the sediment accumulation rate, resulting in the lateral difference of the shelf-edge trajectory in the study area (Figures 10 and 11).

Qiongdongnan Basin is located between the Red River fault zone, Xisha Trough fault zone, and west margin fault zone of the South China Sea, with a complex structure and faults. Since Quaternary, the basin has been in a period of accelerated thermal subsidence, and the tectonic movement has weakened. Most of the faults have stopped activities at this time, but some faults still remain active in the slope area [26]. The No. 2 fault zone runs from east to west of QDNB, with a length of about 300 km (Figure 1). Since Quaternary, the northeastern region of the No. 2 fault zone is still active [21]. The regional activity of the No. 2 fault zone also led to the high-angle rising and recession-slump migration patterns of the shelf edge in the northeast of the study area, and the large-scale development of MTDs. Therefore, the regional activities of fault zone No. 2 not only control the trajectory migration of the shelf edge, but also control the type of sedimentary system in the northeastern part of the basin (Figures 10 and 11).

(2) Global sea level change

Since 1.9 Ma, due to the influence of the ice age, the global temperature has dropped, and the formation of the North and South polar ice sheet has led to sea level fall. During this time, the sea level of QDNB underwent fluctuations [56,57]. The vertical evolution of the shelf-edge trajectory in QDNB show strong relation with sea level changes. When the sea level rises, the progradation rate of the shelf-edge trajectory is small, and when the sea level falls, the progradation rate is large (Figures 10 and 11). Since 0.8 Ma, the eccentricity period at the scale of 100 Ka has increased significantly, the fluctuation amplitude of sea level has increased significantly (up to 120 m), the shelf-edge system has repeatedly collapsed on a large scale, and the shelf-edge trajectory is dominated by the high-angle rising type or the recession-slump type.

5.3.2. Source Supply

There are two main provenance supply systems in QDNB, namely the Red River provenance system and the Hainan Island provenance system. The Red River provenance system plays an important role in controlling the shelf-edge trajectory migration in the northwest QDNB. According to the calculation of sedimentation rate and sediment transport of the Red River since the formation of QDNB [55], since the Quaternary, the maximum sediment transport capacity of the Red River is $38 \text{ km}^3/\text{My}$. Since Quaternary, due to the decreasing sedimentation rate of Yinggehai Basin, it has been gradually filled, and the influence range of Red River provenance has gradually increased, with the northwestern part of the basin as a whole being under the influence of the Red River provenance system [33]. Studies on

the distribution patterns of rare earth elements in drilling samples from different regions of QDNB show that the distribution characteristics of rare earth elements in the sediments of northeastern QDNB since Quaternary are almost identical with those in the source region of Hainan Island [24,58]. Therefore, it is believed that the provenance system of Hainan Island dominates the shelf-edge trajectory in the northeast QDNB. Since the Quaternary, the sediment supply of Hainan Island has been increasing, and the sediment transport is within the range of 15–45 km³/My [59].

Since 1.9 Ma, the Red River provenance has entered through the northwest of QDNB [60], and while there are rivers in the southwest of Hainan Island, there are fewer rivers in the southeast. As a result, the sedimentary center of the basin has always been located in the northwest, and the amount of sediment received in the northwest of the study area is much larger than that in the northeast [55,61], resulting in the extreme advance of the shelf-edge system in the northwest of the study area, whose maximum distance is up to 24 km. Due to the small supply of sediment, the shelf-edge trajectory of the northeastern basin is dominated by the high-angle rising type, resulting in little advance of the shelf-edge system (25–500 m), and the instability of sediment accumulation is prone to collapse. It is concluded that provenance supply plays a leading role in the differential evolution of the east and west sides of QDNB [11].

5.3.3. Climate Change

According to the study of Cenozoic palynological assemblages in Qiongdongnan, the climate in the northern part of the South China Sea has gradually changed from hot and humid to cool and dry, and from tropical to subtropical since Quaternary [62,63]. Based on the analysis of sediment records at ODP1145 and ODP1144, it is concluded that the carbonate content at ODP1145 showed a significant decrease at around 1.9 Ma, which may indicate the significant enhancement of the East Asian winter monsoon during this time [31,64]. After about 0.8 Ma, the 100 Ka scale eccentricity period was significantly enhanced in response to the Mid Pleistocene Transition (MPT). Before the Pleistocene climate change, the climate in QDNB was a typical tropical climate [36]. After the transition, the QDNB was affected by the strengthening of the East Asian winter monsoon, the temperature dropped, and the climate changed to subtropical (Figure 11).

The change in the overall climate pattern determines the strength of the provenance supply and indirectly controls the shelf-edge trajectory [36]. Through the comparison of climate change and the shelf-edge trajectory in the study area, it can be found that the accumulation rate of the shelf-edge trajectory will increase with the decrease of temperature and the intensification of the East Asian winter monsoon. After the Mid Pleistocene Transition (MPT) occurred, the sediment flux in the study area increased significantly, resulting in a significant increase in the formation thickness in the study area since 0.8 Ma (Figure 11).

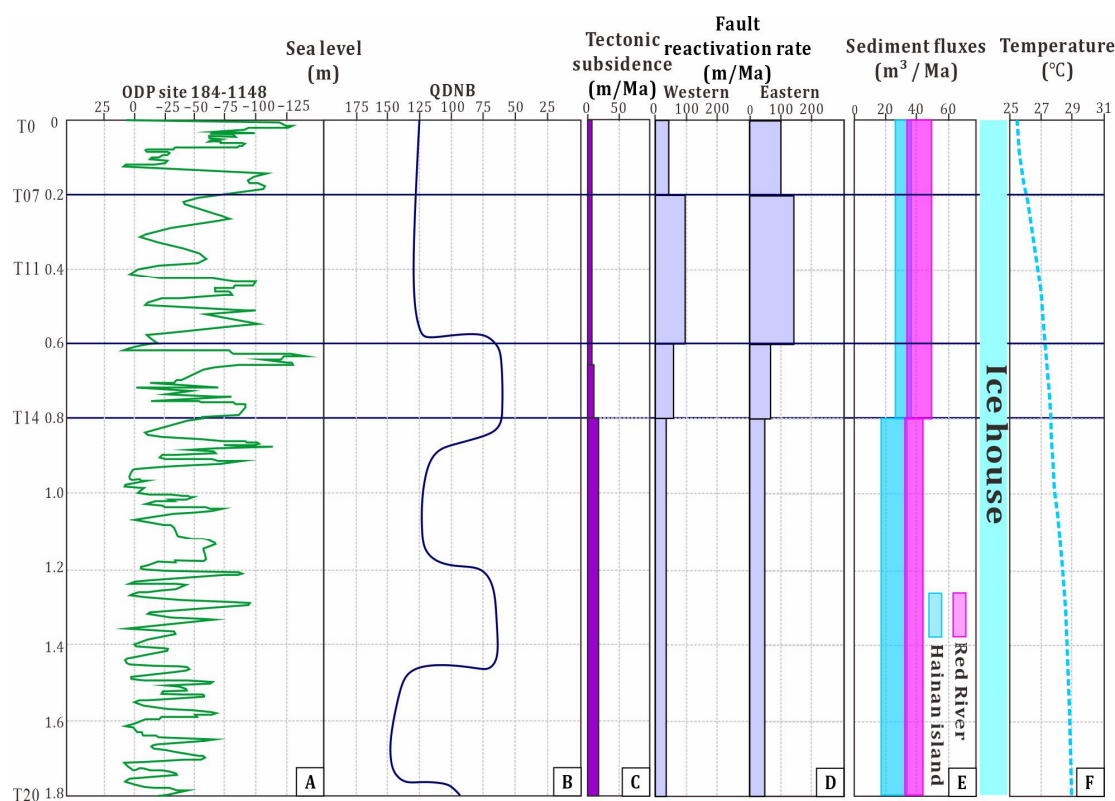


Figure 11. (A) Sea level records in the northern South China Sea (ODP site 184–1148) (green line) from 0 to 1.8 Ma derived from [65,66] (B) Sea level records in the QDNB (deep blue line) from 0 to 1.8 Ma derived from [27]. (C) Tectonic subsidence records in the QDNB (purple rectangle) from 0 to 1.8 Ma derived from [54]. (D) Fault reactivation rate records in the QDNB (brown rectangle) from 0 to 1.8 Ma. (E) Sediment flux of QDNB (blue rectangle represents Hainan Island sources; pink rectangle represents Red River sources) from 0 to 1.8 Ma derived from [20,32–34,36]; (F) temperature curve changes from 0 to 1.8 Ma derived from [16].

6. Conclusions

(1) Through quantitative characterization of Quaternary shelf-edge trajectory migration, four types of shelf-edge trajectory migration have been recognized, including low-angle slow ascending type, medium-angle ascending type, high-angle sharp ascending type, and recession-slump type.

(2) In this study, a new sequence stratigraphic framework based on shelf-edge trajectory migration was established. There are four third-order sequences in the Quaternary, and several system domains (LST, TST, HST) have been identified. During the LST period, the shelf-edge trajectory was mainly low-angle type, the progradation rate was higher than the accretion rate. In the TST period, the shelf-edge trajectory was mainly regression-slump type, the sea level rose rapidly, leading to shelf-edge sediment instability and collapse, forming MTDs. During the HST period, the shelf-edge trajectory was mainly medium-angle rising type or high-angle sharp rising type, the accretion rate was almost the same as the progradation rate, the sea level rising rate slowed down, and a large amount of sediment accumulated on the shelf edge.

(3) When the canyon in the slope area is small and the downcutting is shallow, and the deep-sea plain area has multi-stage large-scale submarine fan deposits and fewer MTDs, the trajectory angle is $-1^\circ < \alpha < 4^\circ$. When the canyon increases in the continental slope area, and both submarine fan deposits and MTDs appear in the deep-sea plain area, the trajectory angle is $4^\circ < \alpha < 35^\circ$. When the canyon in the continental slope area is less developed but downcutting is deep, the sediments in the deep-sea plain area are mainly large MTDs, and the submarine fan is poorly developed. In this case, the trajectory angle

is $35^\circ < \alpha < 90^\circ$. When the canyon in the continental slope area is almost undeveloped, the sediments in the deep-sea plain area are mainly large MTDs, and the submarine fan is almost undeveloped, the trajectory angle is $90^\circ < \alpha < 150^\circ$.

(4) Since the Quaternary, the temperature in QDNB has been decreasing, the sea level has been falling, and the East Asian winter monsoon has been significantly enhanced, resulting in an overall increase in sediment supply in the study area. However, due to the numerous rivers and rich sources of sediment in the west of Hainan Island, which is not in the subsidence center, a growing shelf-edge slope has developed. In the eastern part, due to fewer rivers, weak provenance system, strong tectonic activity, and subsidence center, a type of destructive shelf-edge slope has developed in the western part of basin.

Supplementary Materials: The following supporting information can be downloaded at: <https://www.mdpi.com/article/10.3390/jmse12112051/s1>, Table S1: Statistics of shelf-edge trajectory parameters in QDNB. A: Accretion, P: Progradation, α : Shelf-edge trajectory. Table S2: Statistics of slope angle parameters in QDNB. ETT: Edge to toe, Rc: Height between edge and toe. Table S3: Statistics of sediment supply parameters in QDNB. A: Accretion, P: Progradation, Ra: Accretion rate, Rp: Progradation rate, Fc: Sediment flux.

Author Contributions: Conceptualization, H.Q.; methodology, C.M.; software, C.M.; validation, C.M.; formal analysis, C.M.; investigation, X.L.; resources, H.Q.; data curation, C.M.; writing—original draft preparation, C.M. and X.L.; writing—review and editing, H.Q.; visualization, C.M.; supervision, H.Q.; project administration, H.Q.; funding acquisition, H.Q. All authors have read and agreed to the published version of the manuscript.

Funding: This research received no external funding. And The APC was funded by Hongjun Qu.

Data Availability Statement: The original contributions presented in this study are included in the article/Supplementary Material. Further inquiries can be directed to the corresponding author.

Conflicts of Interest: The authors declare no conflict of interest.

References

- Helland-Hansen, W.; Martinsen, O.J. Shoreline Trajectories and Sequences; Description of Variable Depositional-Dip Scenarios. *J. Sediment. Res.* **1996**, *66*, 670–688.
- Løseth, T.M.; Helland-Hansen, W. Predicting the Pinchout Distance of Shoreline Tongues. *Terra Nova* **2001**, *13*, 241–248. [[CrossRef](#)]
- Payton, C.E. *Seismic Stratigraphy—Applications to Hydrocarbon Exploration*; American Association of Petroleum Geologists: Tulsa, OK, USA, 1977.
- Steel, R.; Olsen, T. Clinofolds, Clinofold Trajectories and Deepwater Sands. In *Sequence Stratigraphic Models for Exploration and Production: Evolving Methodology, Emerging Models, and Application Histories: 22nd Annual*; SEPM Society for Sedimentary Geology: Tulsa, OK, USA, 2002; pp. 367–380.
- Chenglin, G.; Wang, Y.; Steel, R.J.; Olariu, C.; Xu, Q.; Liu, X.; Zhao, Q. Growth Styles of Shelf-Margin Clinofolds: Prediction of Sand-and Sediment-Budget Partitioning into and across the Shelf. *J. Sediment. Res.* **2015**, *85*, 209–229.
- Tugdual, G.; Rovere, M.; Pellegrini, C.; Cattaneo, A.; Campiani, E.; Trincardi, F. Factors Controlling Margin Instability During the Plio-Quaternary in the Gela Basin (Strait of Sicily, Mediterranean Sea). *Mar. Pet. Geol.* **2021**, *123*, 104767.
- Helland-Hansen, W.; Hampson, G.J. Trajectory Analysis: Concepts and Applications. *Basin Res.* **2009**, *21*, 454–483. [[CrossRef](#)]
- Gemma, E.; Casas, D.; Estrada, F.; Vázquez, J.T.; Iglesias, J.; García, M.; Gómez, M.; Acosta, J.; Gallart, J.; Maestro-González, A. Morphosedimentary Features and Recent Depositional Architectural Model of the Cantabrian Continental Margin. *Mar. Geol.* **2008**, *247*, 61–83.
- Stefano, P.; Scisciani, V.; Helland-Hansen, W.; D’Intino, N.; Reid, W.; Pellegrini, C. Upslope-Climbing Shelf-Edge Clinofolds and the Stepwise Evolution of the Northern European Glaciation (Lower Pleistocene Eridanos Delta System, UK North Sea): When Sediment Supply Overwhelms Accommodation. *Basin Res.* **2020**, *32*, 224–239.
- Si, C.; Steel, R.; Olariu, C.; Li, S. Growth of the Paleo-Orinoco Shelf-Margin Prism: Process Regimes, Delta Evolution, and Sediment Budget Beyond the Shelf Edge. *Bulletin* **2018**, *130*, 35–63.
- Mengnan, L.; Liu, H.; van Loon, A.J.; Xu, J.; Hao, S.; Zhang, Y. Analysis of the Geometric Characteristics of Clinofolds and the Relationship with Shelf-Edge Trajectories of the Plio-Pleistocene Continental Slope in the Qiongdongnan Basin, South China Sea. *Sedimentology* **2023**, *70*, 5–30.
- Chenglin, G.; Steel, R.J.; Wang, Y.; Lin, C.; Olariu, C. Shelf-Margin Architecture Variability and Its Role in Sediment-Budget Partitioning into Deep-Water Areas. *Earth-Sci. Rev.* **2016**, *154*, 72–101.
- Chenglin, G.; Wang, Y.; Zhu, W.; Li, W.; Xu, Q.; Zhang, J. The Central Submarine Canyon in the Qiongdongnan Basin, Northwestern South China Sea: Architecture, Sequence Stratigraphy, and Depositional Processes. *Mar. Pet. Geol.* **2011**, *28*, 1690–1702.

14. Chen Percy, P.H.; Chen, Z.Y.; Zhang, Q.M. Sequence Stratigraphy and Continental Margin Development of the Northwestern Shelf of the South China Sea. *AAPG Bull.* **1993**, *77*, 842–862.
15. Ming, S.; Xinong, X.; Junliang, L.; Tao, J.; Cheng, Z.; Yunlong, H.; Shanshan, T.; Cuimei, Z. Gravity Flow on Slope and Abyssal Systems in the Qiongdongnan Basin, Northern South China Sea. *Acta Geol. Sin. Engl. Ed.* **2011**, *85*, 243–253. [[CrossRef](#)]
16. Si, C.; Steel, R.; Wang, H.; Zhao, R.; Olariu, C. Clinoform Growth and Sediment Flux into Late Cenozoic Qiongdongnan Shelf Margin, South China Sea. *Basin Res.* **2020**, *32*, 302–319.
17. Dawei, W.; Wu, S.; Yao, G.; Lü, F.; Strasser, M. Analysis of Quaternary Mass Transport Deposits Based on Seismic Data in Southern Deep-Water Region of Qiongdongnan Basin, South China Sea. In *Landslide Science for a Safer Geoenvironment*; Springer: Cham, Switzerland, 2014; Volume 3.
18. Yuhong, X.; Zhang, G.; Sun, Z.; Zeng, Q.; Zhao, Z.; Guo, S. Reservoir Forming Conditions and Key Exploration Technologies of Lingshui 17-2 Giant Gas Field in Deepwater Area of Qiongdongnan Basin. *Pet. Res.* **2019**, *4*, 1–18.
19. Tao, J.; Xie, X.; Wang, Z.; Li, X.; Zhang, Y.; Sun, H. Seismic Features and Origin of Sediment Waves in the Qiongdongnan Basin, Northern South China Sea. *Mar. Geophys. Res.* **2013**, *34*, 281–294.
20. Shi, X.; Kohn, B.; Spencer, S.; Guo, X.; Li, Y.; Yang, X.; Shi, H.; Gleadow, A. Cenozoic Denudation History of Southern Hainan Island, South China Sea: Constraints from Low Temperature Thermochronology. *Tectonophysics* **2011**, *504*, 100–115. [[CrossRef](#)]
21. Jianye, R.; Zhang, D.; Tong, D.; Huang, A.; Wang, Y.; Lei, C.; Zuo, Q.; Zhao, Y.; He, W.; Yang, L. Characterising the Nature, Evolution and Origin of Detachment Fault in Central Depression Belt, Qiongdongnan Basin of South China Sea: Evidence from Seismic Reflection Data. *Acta Oceanol. Sin.* **2014**, *33*, 118–126.
22. Cao, L.; Jiang, T.; Wang, Z.; Zhang, Y.; Sun, H. Provenance of Upper Miocene Sediments in the Yinggehai and Qiongdongnan Basins, Northwestern South China Sea: Evidence from Ree, Heavy Minerals and Zircon U–Pb Ages. *Mar. Geol.* **2015**, *361*, 136–146. [[CrossRef](#)]
23. Stefan, N.; Granjeon, D.; Willett, S.; Lin, A.T.-S.; Castelltort, S. Stratigraphic Modeling of the Western Taiwan Foreland Basin: Sediment Flux from a Growing Mountain Range and Tectonic Implications. *Mar. Pet. Geol.* **2018**, *96*, 331–347.
24. Lei, C.; Ren, J. Hyper-Extended Rift Systems in the Xisha Trough, Northwestern South China Sea: Implications for Extreme Crustal Thinning Ahead of a Propagating Ocean. *Mar. Pet. Geol.* **2016**, *77*, 846–864. [[CrossRef](#)]
25. Zhao, Z.; Sun, Z.; Sun, L.; Wang, Z.; Sun, Z. Cenozoic Tectonic Subsidence in the Qiongdongnan Basin, Northern South China Sea. *Basin Res.* **2018**, *30*, 269–288. [[CrossRef](#)]
26. Mao, K.; Xie, X.; Xie, Y.; Ren, J.; Chen, H. Post-Rift Tectonic Reactivation and Its Effect on Deep-Water Deposits in the Qiongdongnan Basin, Northwestern South China Sea. *Mar. Geophys. Res.* **2015**, *36*, 227–242. [[CrossRef](#)]
27. Zhao, Z.; Sun, Z.; Wang, Z.; Sun, Z.; Liu, J.; Zhang, C. The High Resolution Sedimentary Filling in Qiongdongnan Basin, Northern South China Sea. *Mar. Geol.* **2015**, *361*, 11–24. [[CrossRef](#)]
28. Jie, H.; Wan, S.; Xiong, Z.; Zhao, D.; Liu, X.; Li, A.; Li, T. Geochemical Records of Taiwan-Sourced Sediments in the South China Sea Linked to Holocene Climate Changes. *Palaeogeogr. Palaeoclimatol. Palaeoecol.* **2016**, *441*, 871–881.
29. Xiao, X.M.; Xiong, M.; Tian, H.; Wilkins, R.W.; Huang, B.; Tang, Y. Determination of the Source Area of the Ya13-1 Gas Pool in the Qiongdongnan Basin, South China Sea. *Org. Geochem.* **2006**, *37*, 990–1002. [[CrossRef](#)]
30. Huang, H.; Huang, B.; Huang, Y.; Xing, L.; Hui, T. Condensate Origin and Hydrocarbon Accumulation Mechanism of the Deepwater Giant Gas Field in Western South China Sea: A Case Study of Lingshui 17-2 Gas Field in Qiongdongnan Basin. *Pet. Explor. Dev.* **2017**, *44*, 409–417. [[CrossRef](#)]
31. Huang, B.; Tian, H.; Li, X.; Wang, Z.; Xiao, X. Geochemistry, Origin and Accumulation of Natural Gases in the Deepwater Area of the Qiongdongnan Basin, South China Sea. *Mar. Pet. Geol.* **2016**, *72*, 254–267. [[CrossRef](#)]
32. Wan, S.; Li, A.; Clift, P.D.; Jiang, H. Development of the East Asian Summer Monsoon: Evidence from the Sediment Record in the South China Sea since 8.5 Ma. *Palaeogeogr. Palaeoclimatol. Palaeoecol.* **2006**, *241*, 139–159. [[CrossRef](#)]
33. Xiaoming, Z.; Qi, K.; Patacci, M.; Tan, C.; Xie, T. Submarine Channel Network Evolution above an Extensive Mass-Transport Complex: A 3d Seismic Case Study from the Niger Delta Continental Slope. *Mar. Pet. Geol.* **2019**, *104*, 231–248.
34. Cheng, C.; Jiang, T.; Kuang, Z.; Ren, J.; Liang, J.; Lai, H.; Xiong, P. Seismic Characteristics and Distributions of Quaternary Mass Transport Deposits in the Qiongdongnan Basin, Northern South China Sea. *Mar. Pet. Geol.* **2021**, *129*, 105118. [[CrossRef](#)]
35. Wang, Z.; Jiang, T.; Zhang, D.; Wang, Y.; Zuo, Q.; He, W. Evolution of Deepwater Sedimentary Environments and Its Implication for Hydrocarbon Exploration in Qiongdongnan Basin, Northwestern South China Sea. *Acta Oceanol. Sin.* **2015**, *34*, 1–10. [[CrossRef](#)]
36. Zhuo, H.; Wang, Y.; Shi, H.; He, M.; Chen, W.; Li, H.; Wang, Y.; Yan, W. Contrasting Fluvial Styles across the Mid-Pleistocene Climate Transition in the Northern Shelf of the South China Sea: Evidence from 3d Seismic Data. *Quat. Sci. Rev.* **2015**, *129*, 128–146. [[CrossRef](#)]
37. Bilal U, H.; Hardenbol, J.A.; Vail, P.R. Chronology of Fluctuating Sea Levels since the Triassic. *Science* **1987**, *235*, 1156–1167.
38. Li, Q.; Zhong, G.; Tian, J. Stratigraphy and Sea Level Changes. In *The South China Sea: Paleoceanography and Sedimentology*; Springer: Berlin/Heidelberg, Germany, 2009; pp. 75–170.
39. Wei, L.; Alves, T.M.; Wu, S.; Völker, D.; Zhao, F.; Mi, L.; Kopf, A. Recurrent Slope Failure and Submarine Channel Incision as Key Factors Controlling Reservoir Potential in the South China Sea (Qiongdongnan Basin, South Hainan Island). *Mar. Pet. Geol.* **2015**, *64*, 17–30.
40. Vall, P.R. The Stratigraphic Signatures of Tectonics, Eustasy and Sedimentology—an Overview. In *Cycles Events Stratigraphy*; Springer: Berlin/Heidelberg, Germany, 1991; pp. 617–659.

41. Pyles, D.R.; Syvitski, J.P.; Slatt, R.M. Defining the Concept of Stratigraphic Grade and Applying It to Stratal (Reservoir) Architecture and Evolution of the Slope-to-Basin Profile: An Outcrop Perspective. *Mar. Pet. Geol.* **2011**, *28*, 675–697. [[CrossRef](#)]
42. Rotzien, J.R.; Caldwell, R.L.; Goggin, L.R. Deepwater Depositional Environments. In *Deepwater Sedimentary Systems*; Elsevier: Amsterdam, The Netherlands, 2022; pp. 251–300.
43. Xiaoming, Z.; Li, M.; Qi, K.; Liu, L.; Hu, G.; Wu, W.; Zhang, W.; Ge, J. Development of a Distinct Submarine Depositional System on a Topographically Complex Niger Delta Slope. *Geol. J.* **2020**, *55*, 3732–3747.
44. Rui, Z.; Chen, S.; Olariu, C.; Steel, R.; Zhang, J.; Wang, H. A Model for Oblique Accretion on the South China Sea Margin; Red River (Song Hong) Sediment Transport into Qiongdongnan Basin since Upper Miocene. *Mar. Geol.* **2019**, *416*, 106001.
45. Jinhua, L.; Peimin, Z.H. Gravity Induced Deposits in the Continental Slope of Qiongdongnan Basin Based on Ultrahigh Resolution Auv Data. *Geol. Sci. Technol. Inf.* **2019**, *38*, 42–50.
46. Pickering, K.T.; Hiscott, R.N. *Deep Marine Systems: Processes, Deposits, Environments, Tectonics and Sedimentation*; John Wiley & Sons: Hoboken, NJ, USA, 2015.
47. Jon R, R.; Hernández-Molina, F.J.; Fomesu, M.; Thieblemont, A. Deepwater Sedimentation Units. In *Deepwater Sedimentary Systems*; Elsevier: Amsterdam, The Netherlands, 2022; pp. 203–249.
48. Hampson, G.J.; Storms, J.E.A. Geomorphological and Sequence Stratigraphic Variability in Wave-Dominated, Shoreface-Shelf Parasequences. *Sedimentology* **2003**, *50*, 667–701. [[CrossRef](#)]
49. Claudio, P.; Asioli, A.; Bohacs, K.M.; Drexler, T.M.; Feldman, H.R.; Sweet, M.L.; Maselli, V.; Rovere, M.; Gamberi, F.; Valle, G.D. The Late Pleistocene Po River Lowstand Wedge in the Adriatic Sea: Controls on Architecture Variability and Sediment Partitioning. *Mar. Pet. Geol.* **2018**, *96*, 16–50.
50. Ramon-Duenas, C.; Rudolph, K.W.; Emmet, P.A.; Wellner, J.S. Quantitative Analysis of Siliciclastic Clinofolds: An Example from the North Slope, Alaska. *Mar. Pet. Geol.* **2018**, *93*, 127–134. [[CrossRef](#)]
51. Pszonka, J.; Žecová, K.; Wendorff, M. Oligocene Turbidite Fans of the Dukla Basin: New Age Data from the Calcareous Nannofossils and Palaeoenvironmental Conditions (Cergowa Beds, Polish–Slovakian Borderland). *Geol. Carpathica* **2019**, *70*, 311–324. [[CrossRef](#)]
52. Pszonka, J.; Wendorff, M.; Godlewski, P. Sensitivity of Marginal Basins in Recording Global Icehouse and Regional Tectonic Controls on Sedimentation. Example of the Cergowa Basin, (Oligocene) Outer Carpathians. *Sediment. Geol.* **2023**, *444*, 106326. [[CrossRef](#)]
53. Anell, I.; Midtkandal, I.; Braathen, A. Trajectory Analysis and Inferences on Geometric Relationships of an Early Triassic Prograding Clinofold Succession on the Northern Barents Shelf. *Mar. Pet. Geol.* **2014**, *54*, 167–179. [[CrossRef](#)]
54. Xi, X.; Müller, R.D.; Ren, J.; Jiang, T.; Zhang, C. Stratigraphic Architecture and Evolution of the Continental Slope System in Offshore Hainan, Northern South China Sea. *Mar. Geol.* **2008**, *247*, 129–144. [[CrossRef](#)]
55. Clift, P.D.; Sun, Z. The Sedimentary and Tectonic Evolution of the Yinggehai–Song Hong Basin and the Southern Hainan Margin, South China Sea: Implications for Tibetan Uplift and Monsoon Intensification. *J. Geophys. Res. Solid Earth* **2006**, *111*, B06405. [[CrossRef](#)]
56. Stow, D.A.V.; Howell, D.G.; Nelson, C.H. Sedimentary, Tectonic, and Sea-Level Controls. In *Submarine Fans and Related Turbidite Systems*; Springer: Berlin/Heidelberg, Germany, 1985; pp. 15–22.
57. Miller, K.G.; Kominz, M.A.; Browning, J.V.; Wright, J.D.; Mountain, G.S.; Katz, M.E.; Sugarman, P.J.; Cramer, B.S.; Christie-Blick, N.; Pekar, S.F. The Phanerozoic Record of Global Sea-Level Change. *Science* **2005**, *310*, 1293–1298. [[CrossRef](#)]
58. Hao, L.; Meng, J.; Zhang, Y.; Yang, L. Pliocene Seismic Stratigraphy and Deep-Water Sedimentation in the Qiongdongnan Basin, South China Sea: Source-to-Sink Systems and Hydrocarbon Accumulation Significance. *Geol. J.* **2019**, *54*, 392–408.
59. Xubiao, L.; Ge, J.; Zhao, X.; Qi, K.; Jones, B.G.; Fang, X. Geochemistry of Quaternary Sediments in the Northwestern South China Sea: Sediment Provenance and Mid-Pleistocene Transition. *Mar. Geol.* **2024**, *477*, 107371.
60. Xu, D.R.; Xia, B.; Li, P.C.; Chen, G.H.; Ma, C.; Zhang, Y.Q. Protolith Natures and U-Pb Sensitive High Mass-Resolution Ion Microprobe (Shrimp) Zircon Ages of the Metabasites in Hainan Island, South China: Implications for Geodynamic Evolution since the Late Precambrian. *Isl. Arc* **2007**, *16*, 575–597. [[CrossRef](#)]
61. Long, V.H.; Clift, P.D.; Schwab, A.M.; Huuse, M.; Nguyen, D.A.; Zhen, S. Large-Scale Erosional Response of SE Asia to Monsoon Evolution Reconstructed from Sedimentary Records of the Song Hong–Yinggehai and Qiongdongnan Basins, South China Sea. *Geol. Soc. Lond. Spec. Publ.* **2010**, *342*, 219–244.
62. Alley, R.B. Wally Was Right: Predictive Ability of the North Atlantic “Conveyor Belt” Hypothesis for Abrupt Climate Change. *Annu. Rev. Earth Planet. Sci.* **2007**, *35*, 241–272. [[CrossRef](#)]
63. Jie, H.; Li, A.; Wan, S. Sensitive Grain-Size Records of Holocene East Asian Summer Monsoon in Sediments of Northern South China Sea Slope. *Quat. Res.* **2011**, *75*, 734–744.
64. Mei, S.; Wang, X.; Zhang, S.; Chu, G.; Su, Y.; Yang, Z. A 20,000-Year High-Resolution Pollen Record from Huguangyan Maar Lake in Tropical–Subtropical South China. *Palaeogeogr. Palaeoclimatol. Palaeoecol.* **2017**, *472*, 83–92.

65. Tian, J.; Zhao, Q.; Wang, P.; Li, Q.; Cheng, X. Astronomically Modulated Neogene Sediment Records from the South China Sea. *Paleoceanography* **2008**, *23*. [[CrossRef](#)]
66. Bates, S.L.; Siddall, M.; Waelbroeck, C. Hydrographic Variations in Deep Ocean Temperature over the Mid-Pleistocene Transition. *Quat. Sci. Rev.* **2014**, *88*, 147–158. [[CrossRef](#)]

Disclaimer/Publisher’s Note: The statements, opinions and data contained in all publications are solely those of the individual author(s) and contributor(s) and not of MDPI and/or the editor(s). MDPI and/or the editor(s) disclaim responsibility for any injury to people or property resulting from any ideas, methods, instructions or products referred to in the content.